Proceedings of the
Annual Stability Conference
Structural Stability Research Council
Toronto, Canada, March 25-28, 2014

Experimental Studies of Cold-Formed Steel Hollow Section Columns at Elevated Temperatures

M. Balarupan[1], M. Mahendran[2]

Abstract

This paper reports the details of an experimental study of cold-formed steel hollow section columns at ambient and elevated temperatures. In this study the global buckling behaviour of cold-formed Square Hollow Section (SHS) slender columns under axial compression was investigated at various uniform elevated temperatures up to 700°C. The results of these column tests are reported in this paper, which include the buckling/failure modes at elevated temperatures, and ultimate load versus temperature curves. Finite element models of tested columns were also developed and their behaviour and ultimate capacities at ambient and elevated temperatures were studied. Fire design rules given in European and American standards including the Direct Strength Method (DSM) based design rules were used to predict the ultimate capacities of tested columns at elevated temperatures. Elevated temperature mechanical properties and stress-strain models given in European steel design standards and past researches were used with design rules and finite element models to investigate their effects on SHS column capacities. Comparisons of column capacities from tests and finite element analyses with those predicted by current design rules were used to determine the accuracy of currently available column design rules in predicting the capacities of SHS columns at elevated temperatures and the need to use appropriate elevated temperature material stress-strain models. This paper presents the important findings derived from the comparisons of these column capacities.

1. Introduction

Cold-formed steel members differ greatly from hot-rolled steel members in shape, as well as strength and deformation properties. The cold working process alters the properties of the steel, resulting in a higher post-forming strength of the cross section by about 20-50% depending on the type of forming and section thickness. Among a variety of steel sections available, hollow sections are preferred for use as columns in buildings due to their architecturally pleasing shape which are also structurally efficient and economic. The higher torsional rigidity of these closed sections increases their structural stability as columns. The structural performance of columns is of prime importance since they are one of the main load bearing elements of a building. Hence when steel hollow sections are designed as load bearing columns, their performance under fire conditions should be considered to avoid serious damage to lives and properties during fire events. But the available fire design rules in the standards are specified mostly for hot-rolled steel columns while past research of cold-formed steel hollow sections under fire conditions has

[1]PhD Researcher, Queensland University of Technology,<manuvidhya.balarupan@student.qut.edu.au>
[2]Professor, Queensland University of Technology, <m.mahendran@qut.edu.au>

mainly focused on hollow sections in-filled with concrete or stainless steel hollow sections due to the low Fire Resistance Rating (FRR) of traditional thin-walled cold-formed steel hollow sections. Recently, thicker cold-formed square and rectangular hollow sections have been introduced in Australia. These hollow sections can therefore be used as heavily loaded compression members without fire protection. Therefore experimental investigations and finite element analyses were undertaken in this study to investigate the flexural buckling behaviour of slender cold-formed steel hollow section columns at uniform elevated temperatures. This paper presents the details and results of this study including comparisons with current fire design rules.

2. Elevated Temperature Column Tests

2.1 Specimen Selection

Square hollow sections (SHS) were chosen since they have a higher probability of being used as columns in practice. Two G450 SHS columns of different thicknesses but with the same external dimensions (65x65x3 and 65x65x6 SHS) were tested. Grade 450 sections were chosen because they would give the highest strength to weight ratio among the commonly used cold-formed steel columns and are likely to be used as bare steel columns without any additional concrete infilling or protection. Fixed end conditions were chosen since perfect pinned end conditions were harder to achieve in the laboratory. A specimen length of 1800 mm was first chosen so that it could be accommodated in the 2m high electric furnace. The section sizes were then chosen in order to achieve the expected global failure mode in each test for the fixed ended columns. Six tests were carried out for 65x65x3 SHS columns at temperatures of 20, 200, 400, 500, 600 and 700°C. But for 65x65x6 SHS columns only three tests were carried out at 500, 600 and 700°C due to the limitations on the strength of loading frames and their connections.

2.2 Test Setup

Elevated temperature column tests were carried out inside a two-segment electric furnace with an internal height of 2m. A special loading set-up was designed and built to test the 1.8m long SHS columns as shown in Fig. 1. The top and bottom loading shafts were made of 253MA stainless steel solid circular rods of 100 mm diameter. This steel is a high temperature resistant material to ensure greater strength and stability at high temperatures up to 1100°C. The shafts had a much greater stiffness than test columns to eliminate any lateral movements at the column ends. The loading frame consisted of two guidance tubes connected to the strong floor and the top beam that were used to apply a vertical load to the test column. The top loading shaft was connected to the top beam using a special arrangement shown in Fig. 2 (a). The shaft was threaded into a 500x500x40 mm plate using a lock nut. Similarly at the bottom of the furnace, the arrangement shown in Fig. 2 (b) was used to provide support to the bottom loading shaft. The thick base plate was connected to the strong-floor to avoid any movement or rotation. The guidance tubes provided lateral restraints and fixity, ensuring the verticality of both loading shafts. A hydraulic jack was placed beneath the bottom shaft as shown in Fig. 2 (b). The ambient temperature test was also conducted with the test column inside the furnace.

Test columns were welded to 20mm thick G450 circular end plates that were bolted to the end plates of the top and bottom loading shafts as shown in Fig. 1 (b). Insulation sheets were placed between the two loading shaft end plates and the column end plates to minimize heat loss to the external environment from test columns so that the temperature along the column length was maintained as uniform as possible.

Figure 1: (a) Overall test set-up (b) Test column

Figure 2: (a) Top loading arrangement (b) Bottom loading arrangement

The compression load was applied using a hydraulic jack, calibrated previously using a pressure transducer. Two thermocouples which were used to measure the interior air temperature were connected to the control panel of the furnace. Three additional thermocouples were also attached to the test column at three locations to measure the steel temperatures during the test. The measurements of these thermo couples ensured that the test column had reached the desired elevated temperature before the axial compression load was applied.

2.3 Test Procedure

Test columns were located between the loading shafts inside the furnace. After placing the insulation sheets between the test column and shafts, the end plates of test column and loading shafts were bolted together to provide a rigid fixed connection. Before the column tests, the initial global imperfections of the test columns were measured.

Axial deformation of the test specimen was measured using an LVDT. But since the LVDT could not be used inside the furnace, it was placed outside the furnace and the vertical movement of the bottom loading shaft was measured using a plate attached between the bottom loading

shaft and the hydraulic jack (refer Fig. 2 (b)). The lateral displacements were measured at the middle of the shaft using two pull type LVDTs in perpendicular directions. Three additional thermocouples were also attached to the specimen. The hydraulic loading system was set-up, following which the thermocouples, the pressure transducer and the LVDTs were connected to the data acquisition system. The furnace door was closed and the steel column was heated to the required temperature by setting the final air temperature in the furnace control panel. After the furnace internal temperature reached the required level, another 20 minutes was allowed for the test column to reach the desired elevated temperature.

During the heating phase, special care was taken to monitor the load applied to the specimen due to thermal expansion effects, and any load developed due to thermal expansion was released. Once the test column had settled at the desired elevated temperature, the load was applied using the hydraulic pump until failure while recording the applied load and deformations.

2.4 Observations and Results

Only the failure process of the column tested at ambient temperature was able to be viewed since the furnace door was closed during the elevated temperature tests. The increase in load and axial and lateral deformations were monitored and the failure was determined based on the drop in applied load. In the initial stage, only the axial deformation was noticeable with minimal lateral deformations. Higher lateral deformations were observed near the column failure. Fig.3 shows the typical load versus axial and lateral deformation curves.

Figure 3: Typical failure of tested columns

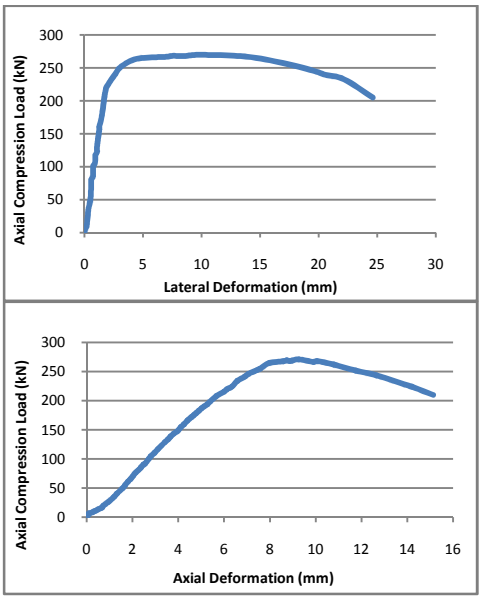

Figure 4: Load vs. Deformation curves

All the test columns failed in flexural buckling as shown in Fig.4. Since they were made of SHS, their failure was not restricted to any particular direction, ie. not even parallel to the column faces. The column failures occurred in random directions at different angles to the column faces. These observations in relation to the failure direction indirectly confirm that the test set-up including the loading alignment used did not cause any undesirable effects such as loading eccentricity. The flexural buckling failure direction was most likely decided by the initial global imperfection of test columns. The failure loads of tested columns are given in Table 1.

Table 1: Failure loads and modes of test columns

SHS section	Temperature (°C)	Failure load (kN)	Failure mode
65x65x3	20	277.6	Flexural buckling
	200	271.9	Flexural buckling
	400	229.2	Flexural buckling
	500	151.3	Flexural buckling
	600	93.2	Flexural buckling
	700	37.1	Flexural buckling
65x65x6	500	298.8	Flexural buckling
	600	179.4	Flexural buckling
	700	72.0	Flexural buckling

3. Finite Element Analyses and Comparisons with Test Results

The tested columns were modelled using the pre-processor MSC PATRAN and analysed using the Finite Element Analysis (FEA) software ABAQUS. For the FEA, the mechanical properties of steel such as the yield strength and the Young's modulus as well as the stress-strain curves are needed at ambient and elevated temperatures. They were determined at ambient temperature by conducting tensile tests on coupons extracted from the flat faces (not welded faces) of the same sections used for test columns. The mechanical property reduction factors and stress-strain material models proposed by other researchers and design codes were then used to obtain the elevated temperature mechanical properties of steel used in making the test columns used here.

3.1 Finite Element Analysis

3.1.1 Modelling of Tested Columns

Cold-formed steel hollow sections are usually thicker than other thin-walled cold-formed profiles and thus their larger rounded corners cannot be neglected. Therefore, the SHS columns were modelled with rounded corners in this research for greater accuracy. Fixed end conditions were used in the column tests. Hence the FE models were also developed with fixed end support conditions using Multiple Point Constraints (MPCs). The translations and rotations of the MPC at one end of the column were restrained in all directions, and on the other side, the translation of the column end in the direction parallel to the column length was released with all others restrained. Strain-hardening models were used for higher accuracy compared to perfect plastic models. Details of the ambient and elevated temperature mechanical properties and associated stress-strain models used are given in Section 3.2.3. The developed models were used first in a bifurcation buckling analysis and then in a nonlinear analysis that included appropriate initial imperfections and residual stresses.

3.1.2 Column Imperfections

Column imperfections in steel sections are generally caused by their manufacturing, and stacking and handling processes. The global imperfections of test columns were measured before they were tested. The local imperfections were neglected since the expected failure mode of the chosen compact SHS section columns was flexural buckling. The measured global imperfections were less (<0.5mm) than the accepted limiting global imperfection value of L/1000. Hence a global imperfection value of 1.8 mm (1800/1000) was used in the nonlinear finite element analysis to account for any other imperfections and deviations in testing including possible

loading eccentricities. The first buckling mode derived from the bifurcation buckling analysis was used to model the column imperfection shape and the chosen magnitude of 1.8mm.

3.1.3 Residual Stresses

Bending and membrane residual stresses are created in cold-formed steel hollow sections by the cold-forming process and uneven cooling due to welding process, respectively. The distribution of these residual stresses also varies between sections with similar dimensions, but with different production processes such as press braking, direct roll-forming and indirect roll-forming. Cold-formed sections gain additional strength during the cold-forming process. However, at elevated temperatures, they tend to lose the additional strength gained due to cold-forming. Hence it is important to include the residual stresses in the model to monitor the behaviour of cold-formed steel sections at elevated temperatures although the effect of residual stresses may be relatively small as concluded by past research.

Based on the residual stress models proposed by previous researchers (Key and Hancock, 1993, Li et al., 2009, Sully and Hancock, 1996, Tong et al., 2012), an idealized residual stress model is proposed for the FE models of SHS columns used in this research. Figs. 5 and 6 show the idealized residual stress models of flexural and membrane residual stresses used in this research.

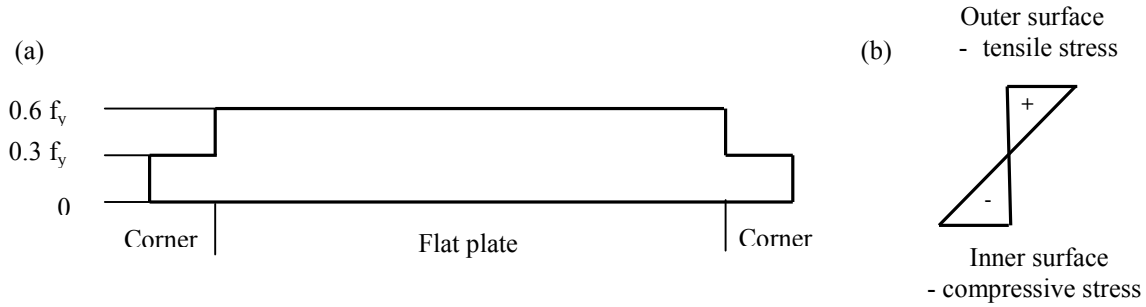

Figure 5: Proposed idealized flexural residual stress model for indirect roll-formed SHS
(a) Distribution along one face (b) Distribution across the thickness

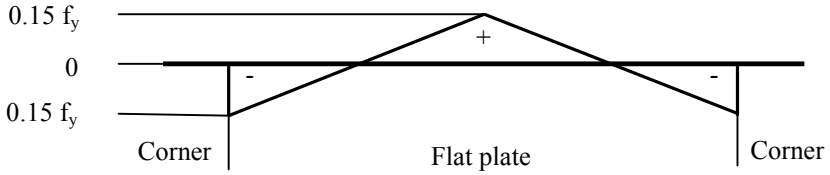

Figure 6: Idealized membrane residual stress model for indirect roll-formed SHS
- distribution along one face

For indirect roll-formed SHS, the corner region has a lower value of flexural residual stress compared to flat plates. A flexural residual stress value of 0.6 times the yield stress is provided in the flat plate areas of SHS and half this value is given in the corner regions based on the models of Key and Hancock (1996) and Sully and Hancock (1993). The membrane residual stress model is proposed for a face of the section without welds, and a maximum value of 0.15 times the yield stress is provided as shown in Fig. 6. The bending residual stresses vary across the thickness as shown in Fig. 5, with equal tensile and compressive stresses on the outer and inner surfaces, respectively, while membrane residual stresses have a uniform value across the thickness.

The residual stresses measured by Li et al. (2009) for indirect roll-formed square hollow sections validate the model by Key and Hancock (1993) and support the values and distribution adopted for the idealized model for this research when the membrane and bending stresses are calculated from the total residual stress measured. The researches mentioned above were all conducted on thin-walled cold-formed hollow sections. The model proposed by Tong et al. (2012) for longitudinal bending residual stresses in cold-formed hollow sections with thicker walls does not vary much from the idealized model proposed here. Hence the proposed model in this paper can be considered to be applicable for sections with thick walls (>6mm) also.

Residual stresses tend to reduce in steel sections with increasing temperature. The rate of residual stress reduction can vary depending on the type of steel section. In this analysis, the model proposed by Lee (2004) was used to determine the reduction in residual stresses with increasing temperature. Table 2 presents the residual stress reduction factors (r) for temperatures (T) from 20 to 700℃ based on Eq.1 proposed by Lee (2004).

$$r = 1.0181 - 0.00128T \quad (1)$$

Table 2: Residual stress reduction factors at elevated temperatures

Temperature T (℃)	20	200	400	500	600	700
Reduction factor (r)	1	0.76	0.51	0.38	0.25	0.13

Table 3: Ambient temperature mechanical properties of tested sections in MPa

Section	0.2% proof stress	Stress at 2% strain	Young's modulus
65x65x3 SHS	463	512	206000
65x65x6 SHS	486	534	197360

Table 4: Mechanical property reduction factors at elevated temperatures

Steel temperature θ_a(℃)	EC3-1.2 (2005) Class 1, 2 and 3			Outinen and Makelainen (2002)			Dolamune Kankanamge & Mahendran (2011)		EC3-1.2 (ECS, 2005) Class 4		ANSI/AISC 360-10 (ASI, 2010)	
	$k_{y,\theta}$	$k_{p,\theta}$	$k_{E,\theta}$	$k_{y,\theta}$	$k_{p,\theta}$	$k_{E,\theta}$	$k_{y,\theta}$	$k_{E,\theta}$	$k_{y,\theta}$	$k_{E,\theta}$	$k_{y,\theta}$	$k_{E,\theta}$
20	1.0	1.0	1.0	1.0	0.85	1.0	1.0	1.0	1.0	1.0	1.0	1.0
100	1.0	1.0	1.0	1.0	0.85	1.0	1.00	0.93	1.0	1.0	1.0	0.99
200	1.0	0.806	0.90	0.97	0.78	0.90	0.99	0.85	0.89	0.90	1.0	0.90
300	1.0	0.613	0.80	0.95	0.65	0.80	0.95	0.72	0.78	0.80	1.0	0.80
400	1.0	0.42	0.70	0.85	0.55	0.70	0.69	0.58	0.65	0.70	0.998	0.70
500	0.78	0.36	0.60	0.65	0.30	0.60	0.39	0.45	0.53	0.60	0.756	0.55
600	0.47	0.18	0.31	0.32	0.12	0.31	0.11	0.31	0.30	0.31	0.487	0.34
700	0.23	0.075	0.13	0.18	0.07	0.13	0.07	0.18	0.13	0.13	0.263	0.17

Note: $k_{y,\theta}$, $k_{E,\theta}$, $k_{p,\theta}$ are the elevated temperature reduction factors for yield strength, Young's modulus and the proportional limit.

3.1.4 Mechanical Properties at Elevated Temperatures

Tested columns were analysed by using four cases of elevated temperature mechanical properties and stress-strain models as proposed by various researchers and standards. These combinations are shown next. For the ambient temperature model, the yield strength, Young's modulus and the stress-strain curve obtained from the tensile coupon tests were used. The mechanical properties of the two tested SHS sections at ambient temperature are given in Table 3 and the mechanical property reduction factors used in this paper for the various comparisons are given in Table 4. ABAQUS requires a stress-strain relationship in terms of true stress and logarithmic plastic strain. Therefore the engineering stress-strain data obtained from tensile coupon tests (σ_{eng} and ε_{eng}) were converted to the true stress and logarithmic plastic strain values (σ_{true} and ε_{pl}) using the following equations (Eqs. 2 and 3).

$$\sigma_{true} = \sigma_{eng}(1 + \varepsilon_{eng}) \tag{2}$$

$$\varepsilon_{pl} = \ln(1 + \varepsilon_{eng}) - \frac{\sigma_{true}}{E} \tag{3}$$

Case 1:

The stress-strain model given in EC3 Part 1.2 (ECS, 2005) for Class 1, 2 and 3 carbon steel sections was used with the elevated temperature reduction factors of yield stress and Young's modulus given in the same design code for the same class of sections. In this model, the yield stress is taken as the stress corresponding to the 2% strain in the stress-strain curve of the steel instead of the 0.2% proof stress which is generally used for cold-formed steels without a definite yield point. Here the Young's modulus and stress at 2% strain from the stress-strain curve of the ambient temperature tensile coupon tests were used with the given reduction factors.

Case 2:

Outinen and Makelainen (2002) conducted tensile coupon tests on hot rolled and cold-formed square hollow sections in steady and transient states at elevated temperatures. They proposed reduction factors for the yield strength, Young's modulus and the proportional limit, which could be used with the stress-strain material model given in EC3 Part 1.2 (ECS, 2005). Hence, in this set of analysis, the EC3 Part 1.2 (ECS, 2005) stress-strain model was used with the elevated temperature reduction factors proposed by Outinen and Makelainen (2002) for the S355J2H structural steel taken from cold-formed 50x50x3 SHS and 80x80x3 SHS. The stress at 2% strain is used as the yield strength since the EC3 Part 1.2 (ECS, 2005) stress-strain model is used.

Case 3:

Dolamune Kankanamge and Mahendran (2011) proposed suitable equations to predict the mechanical properties and stress-strain curves of cold-formed steels at elevated temperatures. In this set of FEA, the mechanical properties (0.2% proof stress and Young's modulus) of steel at elevated temperatures predicted using their equations for high strength steels were used in combination with the stress-strain model proposed by them for cold-formed steels.

Case 4:

In EC3 Part 1.2 (ECS, 2005), elevated temperature reduction factors for yield stress are given separately for Class 4 carbon steel sections in Appendix E. They are the same for both hot-rolled and cold-formed steel sections. The reduction factors are given for the 0.2% proof-stress based yield strength while Young's modulus is the same as for Class 1, 2 and 3 sections. A stress-strain

model is not proposed to be used with these factors in EC3 Part 1.2 (ECS, 2005) and hence the stress-strain model proposed by Dolamune Kankanamge and Mahendran (2011) was used.

3.2 Results and Discussion

The results obtained from FEA simulations of nine column tests using the above mentioned four sets of mechanical properties and stress-strain models are compared with test results. Tables 5 and 6 compare test results with FEA results using these material models. The corresponding curves of ultimate load vs. temperature are shown in Figs. 7 and 8. These results show that FEA results based on the reduction factors and stress-strain models of Dolamune Kankanamge and Mahendran (2011) (Case 3) show larger differences when compared with column test results (overly conservative). For the 65x65x3 SHS columns, the difference is between 15-63% except at 20°C and 200°C. Similar differences are seen for 65x65x6 SHS columns between 500°C and 700°C. Such differences are too high to allow the use of these factors in the modelling and prediction of compression capacities of cold-formed SHS columns. This is mainly due to the much smaller reduction factors at temperatures greater than 300°C. This may be due to the fact that their reduction factors were based on tests of thinner high strength steel sheets.

Table 5: Comparison of column test failure loads with FEA failure loads based on Cases 1 and 2

SHS section	Temperature (°C)	Test results (kN)	FEA Case 1 (kN)	Difference %	FEA Case 2 (kN)	Difference %
65x65x3	20	277.6	291	4.6	291	4.6
	200	271.9	287	5.3	278	2.2
	400	229.2	226	-1.4	218	-4.9
	500	151.3	180	15.9	151	-0.2
	600	93.2	104	10.4	72.6	-22.1
	700	37.1	49.9	25.7	40.5	8.4
65x65x6	500	298.8	322	7.2	271	-9.3
	600	179.4	186	3.6	130	-27.5
	700	72.0	87.6	17.8	72.1	0.1

Table 6: Comparison of column test failure loads with FEA failure loads based on Cases 3 and 4

SHS section	Temperature (°C)	Test results (kN)	FEA Case 3 (kN)	Difference %	FEA Case 4 (kN)	Difference %
65x65x3	20	277.6	291	4.6	291	4.6
	200	271.9	285	4.6	259	-4.7
	400	229.2	197	-14.1	190	-17.1
	500	151.3	114	-24.7	156	3.0
	600	93.2	35	-62.5	87.2	-6.4
	700	37.1	21.9	-41.0	37.5	1.1
65x65x6	500	298.8	211	-29.4	285	-4.6
	600	179.4	64	-64.1	160	-10.8
	700	72.0	40	-44.0	69	-4.7

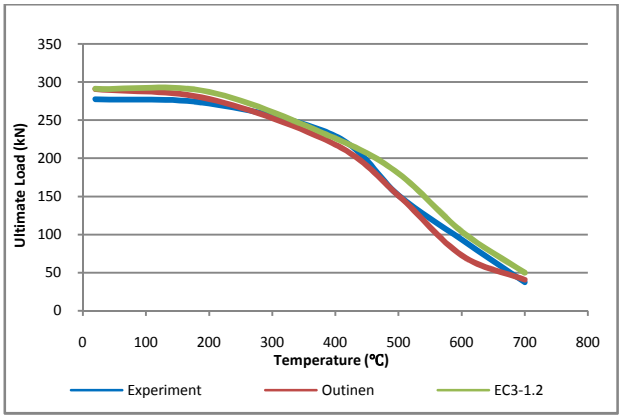

Figure 7 (a): Ultimate load vs. temperature curves- 65x65x3 SHS

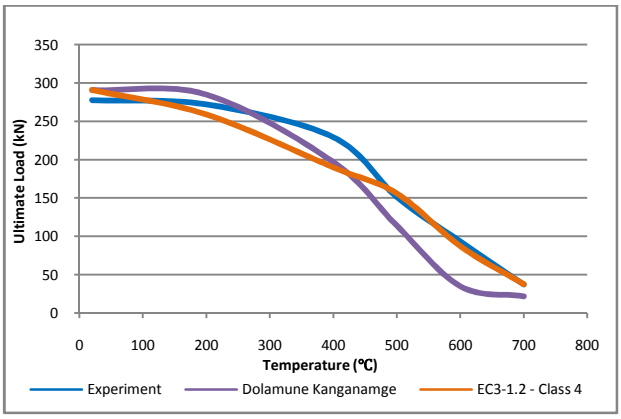

Figure 7 (b): Ultimate load vs. temperature curves- 65x65x3 SHS

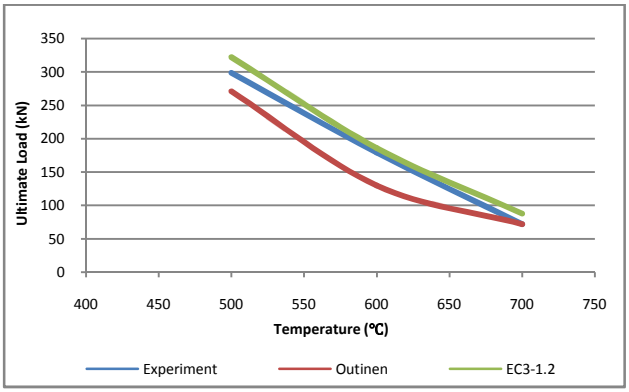

Figure 8 (a): Ultimate load vs. temperature curves- 65x65x6 SHS columns

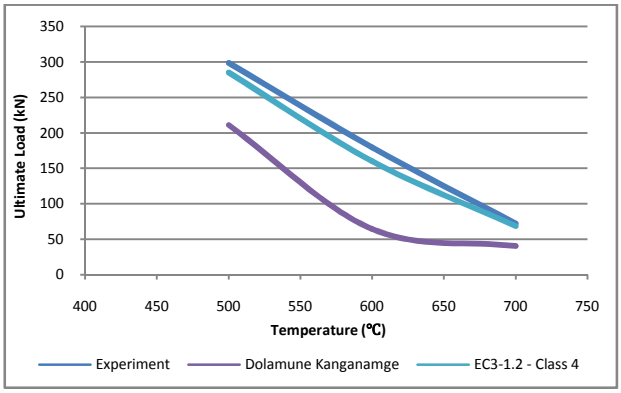

Figure 8 (b): Ultimate load vs. temperature curves- 65x65x6 SHS columns

FEA results based on the elevated temperature reduction factors for Class 4 sections given in EC3 Part 1.2 (Case 4) have smaller differences compared to those for Case 3 with the same stress-strain model. For the 65x65x3 SHS column, the difference is below 7% except at 400°C when it is 17%. FEA results based on the EC3 Part 1.2 (ECS, 2005) reduction factors for Class 1, 2 and 3 sections (Case 1) match well with test capacities at lower temperatures up to 400°C. But for temperatures between 500°C and 700°C the difference is up to 25% and non-conservative. Hence by considering the overall prediction of the failure loads with temperature, the use of the mechanical property reduction factors for Class 1, 2 and 3 steel sections with the stress-strain curve proposed in EC3 Part 1.2 (ECS, 2005) seem to give reasonable results.

Outinen and Makelainen's (2002) reduction factors were proposed specifically based on tensile coupon tests conducted on cold-formed SHS. For 65x65x3 SHS, FEA results match well with test capacities up to 500°C with only about 5% difference. But a 22% difference is seen at 600°C (conservative), which becomes 8.4% at 700°C (non-conservative, but reasonable). A similar pattern is observed for 65x65x6 SHS columns, where a sudden drop is observed at 600°C, which then recovers at 700°C. This set of results prove to be more suitable for the prediction of column capacities of slender cold-formed SHS columns since even the highest difference at 600°C was conservative. Hence it is safe compared to the non-conservative predictions of EC3 Part 1.2 (2005) at higher temperatures. This outcome is mostly due to the smaller reduction factors of Outinen and Makelainen (2002) than in EC3 Part 1.2.

In conclusion, the reduction factors given in EC3 Part 1.2 (ECS, 2005) for Class 1-3 sections and Outinen and Makelainen (2002) appear to give better predictions for slender columns made of compact SHS sections when used in the FE models with EC3 Part 1.2 stress-strain model. These factors can be used in the predictions of column capacities up to 400°C. The reduction factors given in EC3 Part 1.2 for Class 4 sections also appear to give good predictions of SHS column capacities at elevated temperatures. Further experimental studies are needed to accurately determine the elevated temperature mechanical properties of cold-formed steel hollow sections.

4. Column Capacity Predictions using Current Design Rules

In this section, the compression capacities of 65x65x3 and 65x65x6 SHS columns at different elevated temperatures up to 700℃ were calculated using the currently available design rules in the European and American steel design standards. They were then compared with those found from non-linear finite element analyses using ABAQUS and experimental study. Details of the design rules used in this study are given in Appendix A.

4.1 Eurocode 3 Part 1.2 (ECS, 2005)

EC3 Part 1.2 (ECS, 2005) gives design equations to predict the capacities of steel columns at elevated temperatures. These equations use the elevated temperature reduction factors given for the yield strength and Young's modulus together with the non-dimensional slenderness of the columns at ambient temperature (λ). EC3 Part 1.1 (ECS, 2005) was used for this purpose since it is recommended for the design of cold-formed steel hollow sections instead of the cold-formed steel standard EC3 Part 1.3 (ECS, 2006) due to the similar structural behavioural characteristics of hot-rolled and hollow steel sections.

Table 7: Comparison of column capacities predicted using EC3 Part 1.2 design rules with test and FEA results

SHS section	Temperature (℃)	Test results (kN)	FEA results (Case 1) (kN)	EC3 Part 1.2 (kN)
65x65x3	20	277.6	291	214.6
	200	271.9	287	207.1
	400	229.2	226	187.8
	500	151.3	180	152.3
	600	93.2	104	86.0
	700	37.1	49.9	39.1
65x65x6	20	-	523	373.9
	200	-	525	358.2
	400	-	403	318.4
	500	298.8	322	260.3
	600	179.4	186	145.1
	700	72.0	87.6	65.1

Table 7 compares the column capacities of 65x65x3 and 65x65x6 SHS columns of 1.8m length with fixed end conditions calculated using the design equations given in EC3 Part 1.2 (2005) with test capacities and FEA capacities using the same reduction factors (Case 1). It is evident that although the same reduction factors were used, the column capacities calculated using the

design equations give conservative results than FEA and test results except after 500°C for 65x65x3 SHS columns. Even at 20°C, the fire equations predicted a lower capacity compared to those given for general design in EC3 Part 1.1 (2005). A more severe imperfection factor α is included in the fire equations, which provides a higher safety margin in fire conditions.

4.2 ANSI/AISC 360-10 (AISC, 2010)

This American standard of specifications for structural steel buildings provides design rules to calculate the nominal compressive strengths of columns at elevated temperatures. This standard is not recommended for the design of cold-formed steel sections other than hollow structural sections (HSS) with thickness less than 25mm. The column capacities calculated using the fire equations given in ANSI/AISC 360-10 are compared with test results in Table 8.

Table 8: Comparison of column capacities predicted using the ANSI/AISC 360-10 design rules with test results

SHS section	Temperature (°C)	Test results (kN)	ANSI/AISC 360-10 (kN)
65x65x3	20	277.6	208.8
	200	271.9	203.7
	400	229.2	190.1
	500	151.3	145.7
	600	93.2	92.6
	700	37.1	48.9
65x65x6	500	298.8	255.7
	600	179.4	162.3
	700	72.0	85.5

In this standard also, it was observed that the fire equations gave a smaller capacity at 20°C than the ambient temperature compression capacity equations in the same code, providing a higher safety margin. The calculated values remain conservative up to 500°C, but become non-conservative at 700°C. This could be due to the larger reduction factors at high temperatures.

4.3 Direct Strength Method (DSM)

The DSM based design rules proposed by Schafer (2001) for the prediction of cold-formed steel column capacities are included in AISI S100-07 (AISI, 2007) and AS/NZS 4600 (SA, 2005). The four different material models of mechanical property reduction factors at elevated temperatures considered in Section 3 were used with DSM based design equations. Elastic buckling load was taken from the bifurcation FEA using ABAQUS, while the ultimate load was then calculated using the DSM design equations. The 0.2% proof stress given in Table 3 was used as the yield strength in all the DSM design calculations. For elevated temperatures, the reduction factors in Table 4 were used to calculate the yield strength and Young's modulus at relevant temperatures.

Tables 9 and 10 results show that DSM design equations using the elevated temperature mechanical property reduction factors in Cases 1 to 4 are not able to predict the SHS column capacities. They also show that DSM predictions using the reduction factors proposed by Dolamune Kankanamge and Mahendran (2011) and EC3 Part 1.2 (2005) for Class 4 sections give variations similar to those observed in the comparison of test and FEA results (Table 6). But the DSM capacities predicted using the factors of Outinen and Makelainen (2002) and EC3 Part

1.2 (2005) for Class 1-3 sections show different variations to those observed in the comparison of test and FEA results (Table 5). DSM predictions only use the reduction factors and not the stress-strain model, and this is why there are these observed differences. It appears that DSM design equations support the use of the stress-strain model as used under Cases 3 and 4.

Table 9: Comparison of test results with capacities from DSM design equations (Cases 3 and 4)

Section	Temperature (°C)	Test results (kN)	DSM (Case 3)		DSM (Case 4)	
			Ultimate load (kN)	% Difference	Ultimate load (kN)	% Difference
65x65x3	20	277.6	293.96	5.6	293.96	5.6
	200	271.9	285.09	4.6	261.99	-3.6
	400	229.2	199.00	-13.2	192.82	-15.9
	500	151.3	116.64	-22.9	158.13	4.3
	600	93.2	35.10	-62.3	88.55	-5.0
	700	37.1	22.21	-40.1	38.21	2.9
65x65x6	500	298.8	212.93	-28.7	288.60	-3.4
	600	179.4	65.17	-63.7	161.18	-10.2
	700	72	41.17	-42.8	69.48	-3.5

Table 10: Comparison of test results with capacities from DSM design equations (Cases 1 and 2)

Section	Temperature (°C)	Test results (kN)	DSM (Case 1)		DSM (Case 2)	
			Ultimate load (kN)	% Difference	Ultimate load (kN)	% Difference
65x65x3	20	277.6	293.96	5.6	293.96	5.6
	200	271.9	289.83	6.2	282.33	3.7
	400	229.2	278.36	17.7	243.15	5.7
	500	151.3	220.70	31.5	189.06	20.0
	600	93.2	129.38	28.0	93.68	0.5
	700	37.1	61.31	39.5	50.39	26.4
65x65x6	500	298.8	397.43	24.8	342.83	12.8
	600	179.4	231.36	22.5	170.16	-5.6
	700	72	108.74	33.8	90.48	20.4

Next, the DSM results using the four sets of reduction factors (Cases 1 to 4) are compared with FEA results. In Tables 11 and 12, the DSM results using the four sets of reduction factors are compared with FEA results using the same reduction factors in combination with the stress-strain material model of Dolamune Kankanamge and Mahendran (2011). This stress-strain model was chosen to represent a strain-hardening material model for cold-formed steel. “Cases 1 and 2 modified” in Table 12 indicates that FEA results are based on the stress-strain model of Dolamune Kankanamge and Mahendran (2011) and the reduction factors used in Cases 1 and 2.

Table 11: Comparison of column capacities from DSM with FEA results based on Cases 3 and 4 reduction factors and Dolamune Kankanamge and Mahendran's (2011) stress-strain model

SHS Section	Temperature (°C)	Case 3			Case 4		
		DSM (kN)	FEA (kN)	% Difference	DSM (kN)	FEA (kN)	% Difference
65x65x3	20	293.96	291	-1.0	293.96	291	-1.0
	200	285.09	285	-0.1	261.99	259	-1.1
	400	199.00	197	-1.0	192.82	190	-1.5
	500	116.64	114	-2.3	158.13	156	-1.3
	600	35.10	35.0	-0.3	88.55	87.2	-1.5
	700	22.21	21.9	-1.4	38.21	37.5	-1.9
65x65x6	20	534.50	523	-2.2	534.50	523	-2.2
	200	515.60	520	0.9	476.54	478	0.3
	400	359.54	359	-0.2	351.40	348	-1.0
	500	212.93	211	-0.9	288.60	285	-1.3
	600	65.17	64	-1.2	161.18	160	-0.7
	700	41.17	40	-2.1	69.48	69	-1.3

Table 12: Comparison of column capacities from DSM with FEA results based on Cases 1 and 2 reduction factors and Dolamune Kankanamge and Mahendran's (2011) stress-strain model

SHS Section	Temperature (°C)	Case 1 modified			Case 2 modified		
		DSM (kN)	FEA (kN)	% Difference	DSM (kN)	FEA (kN)	% Difference
65x65x3	20	293.96	293	-1.0	293.96	291	-1.0
	200	289.83	287	-1.0	282.33	281	-0.5
	400	278.36	279	0.2	243.15	240	-1.3
	500	220.7	220	-0.3	189.06	187	-1.1
	600	129.38	129	-0.3	93.68	92.8	-0.9
	700	61.31	61.9	1.0	50.39	50.4	0.1
65x65x6	20	534.50	523	-2.2	534.50	523	-2.2
	200	525.10	528	0.6	512.07	513	0.2
	400	499.17	507	1.5	439.05	441	0.4
	500	397.43	400	0.6	342.83	341	-0.5
	600	231.36	237	2.4	170.16	169	-0.7
	700	108.74	110	1.2	90.48	91.6	1.2

The above comparison shows that any mechanical property reduction factors used with the DSM based design rules give good comparisons with FEA predictions. The difference is less than 3% for all four sets of reduction factors with the same stress-strain model of Dolamune Kankanamge and Mahendran (2011). From these comparisons, it appears that the current DSM based design equations include the effects of non-linear stress-strain characteristics at elevated temperatures as proposed by the stress-strain models of Dolamune Kankanamge and Mahendran (2011).

Similarly in Table 13, the reduction factors given in EC3 Part 1.2 (ECS, 2005) for Class 1, 2 and 3 sections and Outinen and Makelainen (2002) for cold-formed steel hollow sections were used in combination with the stress-strain model in EC3 Part 1.2 (ECS, 2005) in obtaining FEA capacities, which were then compared with DSM predictions using the same reduction factors. This comparison was made to check the validity of these reduction factors with other stress-strain models since these reduction factors were proposed to be used with EC3 Part 1.2 stress-strain models and based on 2% strain based yield stress along with proportional limit factors.

Table 13: Comparison of column capacities from DSM with FEA results using EC3 Part 1.2 stress-strain model

Section	Temperature (°C)	Case 1			Case 2		
		DSM (kN)	FEA (kN)	% Difference	DSM (kN)	FEA (kN)	% Difference
65x65x3	20	293.96	291	-1.0	293.96	291	-1.0
	200	289.83	287	-1.0	282.33	278	-1.0
	400	278.36	226	-18.8	243.15	218	-18.8
	500	220.70	180	-18.4	189.06	151	-18.4
	600	129.38	104	-19.6	93.68	72.6	-19.6
	700	61.31	49.9	-18.6	50.39	40.5	-18.6
65x65x6	20	534.50	523	-2.2	534.50	523	-2.2
	200	525.10	525	-0.1	512.07	508	-0.8
	400	499.17	403	-19.3	439.05	397	-9.6
	500	397.43	322	-19.0	342.83	271	-21.0
	600	231.36	186	-19.6	170.16	130	-23.6
	700	108.74	87.6	-19.4	90.48	72.1	-20.3

In the above table, the DSM predictions do not agree with the results from FEA conducted using the EC3 Part 1.2 (ECS, 2005) stress-strain model for temperatures greater than 200°C. This may be because the proportional limit factors are included in FEA, but not in the DSM capacity calculations. Hence comparisons in Tables 11 to 13 show that not only suitable elevated temperature reduction factors of yield strength and Young's modulus must be used, but also the effects of non-linear stress-strain characteristics at elevated temperatures should be included in order to accurately predict the capacities of SHS columns at elevated temperatures.

5. Conclusions

This paper describes the details of an experimental investigation on the flexural buckling behavior and capacities of cold-formed steel hollow section columns at ambient and elevated temperatures up to 700°C, and presents the results. It also describes the development of finite element models to simulate the behaviour of tested columns at ambient and elevated temperatures. Experimental results were compared with FEA results, which were conducted using different sets of mechanical property reduction factors and stress-strain models for steel at elevated temperatures as proposed by different researchers and standards. The mechanical property reduction factors proposed by Outinen and Makelainen (2002) for cold-formed steel hollow sections used with the stress-strain model given in EC3 Part 1.2 (ECS, 2005) gives the predictions closest to the test results out of the four sets considered. The reduction factors given

in EC3 Part 1.2 (ECS, 2005) for Class 1 to 3 sections also give reasonable predictions, but at higher temperatures (>400°C), the results were non-conservative. The reduction factors given in EC3 Part 1.2 for Class 4 sections also appear to give good predictions of SHS column capacities at elevated temperatures. However, further investigations are needed to develop a model for the elevated temperature mechanical properties of the steel used in high strength cold-formed SHS.

The predictions of column capacities based on the design equations given in EC3 Part 1.2, ANSI/AISC 360-10 and DSM varied significantly compared with test column capacities. The DSM capacity predictions agreed well with FEA capacities for all the four sets of reduction factors when used with Dolamune Kankanamge and Mahendran's (2011) stress-strain model. But there was poor agreement when they were compared with FEA capacities obtained using the reduction factors of Outinen and Makelainen (2002) and EC3 Part 1.2 for Class 1-3 sections with the stress-strain model given in EC3 Part 1.2. These comparisons of predicted design capacities with test and FEA capacities indicate that accurate elevated temperature reduction factors of yield strength and Young's modulus and the effects of non-linear stress-strain characteristics at elevated temperatures must be included with suitable column capacity design equations in order to accurately predict the capacities of slender SHS columns at elevated temperatures.

References

American Institute of Steel Construction. (2010). "ANSI/AISC 360: Specification for Structural Steel Buildings." Chicago, USA.

American Iron and Steel Institute. (2007). "AISI S100: North American Specification for the Design of Cold-Formed Steel Structural Members." Chicago, USA.

Dolamune Kankanamge, N. Mahendran, M. (2011). "Mechanical properties of cold-formed steels at elevated temperatures." *Thin-Walled Structures,* 49, 26-44.

EN 1993-1-1. (2005). "Eurocode 3: Design of Steel Structures. Part 1-1: General Rules and rules for buildings." European Committee for Standardization, Brussels.

EN 1993-1-2. (2005). "Eurocode 3: Design of steel structures. Part 1-2: General rules-Structural fire design." European Committee for Standardization, Brussels.

EN 1993-1-3. (2006). "Eurocode 3: Design of steel structures. Part 1-3: General rules-Supplementary rules for cold-formed members and sheeting." European Committee for Standardization, Brussels.

Key, P. W., and Hancock, G.J. (1993). "A Theoretical Investigation of the Column Behaviour of Cold-formed Square Hollow Sections." *Thin-Walled Structures*, 16, 31-64.

Lee, J. (2004). "Local Buckling Behaviour and Design of Cold-Formed Steel Compression Members at Elevated Temperatures." PhD Thesis, Queensland University of Technology, Brisbane, Australia.

Li, S.H., Zeng, G., Ma, Y.F., Guo, Y.J., Lai, X.M. (2009). "Residual Stresses in Roll-formed Square Hollow Sections." *Thin-Walled Structures*, 47, 505–513.

Outinen, J., Makelainen, P. (2002). "Mechanical Properties of Structural Steel at Elevated Temperatures and after Cooling Down." *Second International Workshop-Structures in Fire*, Christchurch.273-290.

Schafer, B.W., (2001). "Thin-walled column design considering local, distortional and Euler buckling." Structural Stability Research Council, Annual Technical Session and Meeting, Ft. Lauderdale, Florida, 419-438.

Standards Australia (SA). (2005). "AS/NZS 4600: Cold-formed Steel Structures." Sydney, Australia.

Sully, R.M., Hancock, G.J. (1996). "Behavior of Cold-Formed SHS Beam-Columns." *Journal of Structural Engineering*, 122, 326-336.

Tong, L., Hou, G., Chen, Y., Zhou, F., Shen, K., Yang, A. (2012). "Experimental Investigation on Longitudinal Residual Stresses for Cold-formed Thick-walled Square Hollow Sections." *Journal of Constructional Steel Research*, 73, 105–116.

Appendix A

This section provides the details of design rules used in calculating the column capacities at elevated temperatures.

A.1 EC3 Part 1.2 (ECS, 2005)

The design buckling resistance ($N_{b,fi,t,Rd}$) at time t of a compression member with a Class 1, Class 2 or Class 3 cross-section with a uniform temperature θ_a is (Eq. A1):

$$N_{b,fi,t,Rd} = \chi_{fi} A k_{y,\theta} f_y / \gamma_{M,fi} \tag{A1}$$

where,

$k_{y,\theta}$= Yield strength reduction factor at temperature θ_a reached at time t

χ_{fi} = The reduction factor for flexural buckling in the fire design situation

$$\chi_{fi} = \frac{1}{\phi_\vartheta + \sqrt{\phi_\vartheta^{\,2} - \bar{\lambda}_\vartheta^2}} \tag{A2}$$

$$\phi_\vartheta = \frac{1}{2}[1 + \alpha \bar{\lambda}_\vartheta + \bar{\lambda}_\vartheta^{\,2}] \tag{A3}$$

$$\alpha = 0.65\sqrt{235 / f_y} \tag{A4}$$

The non-dimensional slenderness for the temperature θ_a,

$$\bar{\lambda}_\vartheta = \bar{\lambda}[k_{y,\vartheta} / k_{E,\vartheta}]^{0.5} \tag{A5}$$

where,

$k_{E,\vartheta}$= Reduction factor for the slope of the linear elastic range at temperature $\theta_a$reached at time t.

$$\bar{\lambda} = \sqrt{\frac{A_{eff} f_y}{N_{cr}}} \tag{A6}$$

where,

A_{eff} = Effective area

N_{cr} = Critical elastic buckling load based on the gross sectional properties

A.2 ANSI/AISC 360-10 (AISC, 2010)

The critical stress for the determination of the nominal compressive strength at temperature T is calculated as (Eq. A7):

$$F_{cr}(T) = \left[0.42^{\sqrt{F_y(T) / F_e(T)}} \right] F_y(T) \tag{A7}$$

where,
$F_y(T)$ is the yield strength at temperature T and $F_e(T)$ is the critical elastic buckling stress

$$F_e(T) = \frac{\pi^2 E(T)}{\left(KL/r\right)^2} \quad \text{(A8)}$$

A.2 Direct Strength Method (DSM) (AISI, 2007)
The DSM is based on Eqs. A9 to A11. The nominal axial strength (P_n) is taken as the minimum of flexural, torsional or flexural torsional buckling load (P_{ne}), *local buckling load* ($P_{n\lambda}$) or distortional buckling load (P_{nd}).

For flexural, torsional or flexural-torsional buckling,

For $\lambda_c \leq 1.5$, $$P_{ne} = \left(0.658^{\lambda_c^2}\right) P_y \quad \text{(A9)}$$

For $\lambda_c > 1.5$, $$P_{ne} = \left(\frac{0.877}{\lambda_c^2}\right) P_y \quad \text{(A10)}$$

where,

$$\lambda_c = \sqrt{P_y / P_{cre}} \quad \text{(A11)}$$

$P_y = A_g F_y$
A_g = Gross sectional area
F_y= Yield stress
P_{cre} = Minimum of the critical elastic column buckling load in flexural, torsional or flexural-torsional buckling.